Defects in Catalysis

DOI: 10.1002/anie.201404022

The Virtue of Defects: Stable Bromine Production by Catalytic Oxidation of Hydrogen Bromide on Titanium Oxide

Maximilian Moser, Izabela Czekaj, Núria López, and Javier Pérez-Ramírez**

Dedicated to the MPI für Kohlenforschung on the occasion of its centenary

© 2014 Wiley-VCH Verlag GmbH & Co. KGaA, Weinheim

Abstract: *Rutile TiO_2 is a heavily investigated oxide with, to date, scarce applications in industrial catalysis. The inactivity of this material in oxidations has been related to its inability to dissociate molecular oxygen. Herein we show how rutile catalyzes the oxidation of HBr to Br_2 through defect states that are introduced during the reaction. The identification of active, stable, and abundant materials for bromine production is key to the future implementation of Br_2-mediated alkane functionalization processes. The catalytic properties of TiO_2 are discussed in comparison to expensive rutile-type oxides, such as RuO_2 and IrO_2, on the basis of surface characterization and molecular modeling.*

In reducible oxides, such as CeO_2 and TiO_2, unavoidable off-stoichiometric compositions control the physico-chemical properties of the materials.[1] These semiconductors can be doped intrinsically by oxygen depletion or extrinsically by partially replacing oxygen by higher (or lower) valence-electron atoms such as F (or N). The extra electrons (or holes) appear at energy levels that are forbidden (occupied) in the stoichiometric material. As the relative position between the active electronic levels of the solid and those of reactants and/or products determines activity, defect states can lead to the discovery of new catalytic properties.

Titania (TiO_2) is one of the most studied oxides both in experimental and theoretical grounds.[2] Rutile, the most common polymorph, shows a relatively low surface area and inert character, and thus its use in industrial catalysis is limited. The recently commercialized RuO_2/TiO_2 catalyst for chlorine recovery by HCl oxidation (Deacon reaction) is the exception. In this catalyst, rutile TiO_2 plays a decisive role as a carrier, templating the epitaxial growth of the active phase RuO_2.[3] Herein we show that the generation of defect states in rutile TiO_2 turns an inactive semiconductor into an active and stable catalyst for the production of bromine by HBr oxidation ($2\,HBr + 1/2\,O_2 \rightarrow Br_2 + H_2O$, $\Delta H^0 = -1.43$ eV). This reaction comprises an essential step for the realization of a bromine-mediated alkane-functionalization process, which is a promising technology to activate C–H bonds[4] leading to large amounts of HBr byproduct that for sustainability purposes needs to be effectively recycled. The catalyzed oxidation of HBr is tightly related to the Deacon reaction.[5,6] Experiments have identified the outstanding performance of RuO_2 for the oxidation of HX (X = Cl, Br).[5] In fact, computational screening based on density functional theory (DFT) have indicated that the closest point to the maximal activity for rutile materials is RuO_2.[6] However, ruthenium-based catalysts present a clear drawback for a widespread implementation owing to ruthenium's relatively high and fluctuating price. This situation has triggered the search for more cost-effective and abundant catalytic materials for halogen production. Unfortunately, theoretical studies also concluded that other rutile-type materials are comparatively inactive. For example, stoichiometric TiO_2 was predicted to deliver a 10-order of magnitude lower reaction rate than RuO_2. The highly endergonic nature of oxygen dissociation over defect-free TiO_2 rutile was put forward as the reason for its inactivity.[6] Indeed theoretical studies have shown that the surface of stoichiometric TiO_2 is unable to dissociatively adsorb O_2.[6,7] Several authors[7] have identified that the adsorption of O_2 can be 'switched on' provided that oxygen vacancies exist in the material. However, under oxygen-rich environments, vacancies can be healed,[8] thus their presence is metastable and TiO_2 is regarded as useless for O_2 activation. In contrast, we have now found that rutile TiO_2 exhibits a remarkable activity and stability for HBr oxidation to Br_2. By means of X-photoelectron spectroscopy and DFT, we rationalize the crucial role of defect states to account for this unprecedented catalytic behavior.

The steady-state activity of bulk rutile-type metal oxide catalysts in HBr and HCl oxidation was studied at different temperatures (Figure 1a). The lower operating temperature

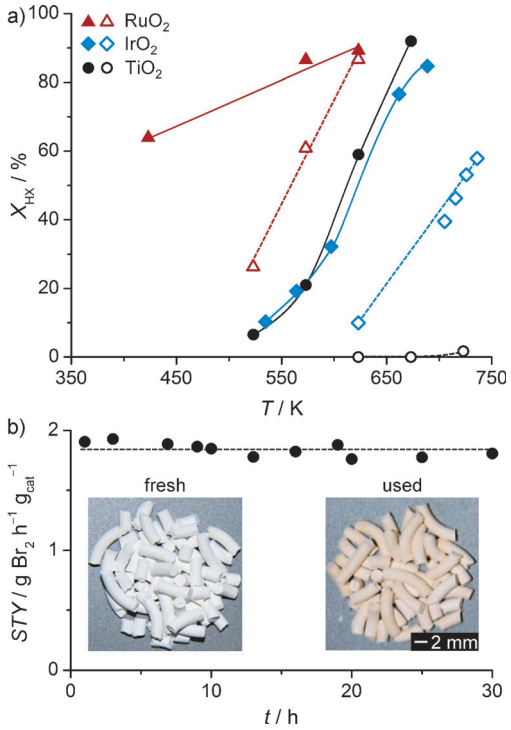

Figure 1. a) Conversion of HX into X_2 (HBr: solid symbols, HCl: open symbols) versus temperature over rutile-type oxides at O_2:HX = 2:1. b) The bromine production measured over TiO_2 extrudates, expressed as the space-time yield in a long-term test. Inset: photographs showing the clear color change of the solid from the characteristic white of fresh TiO_2 to pale yellow upon use in HBr oxidation (the color change occurred instantaneously after exposing the material to the reaction mixture and is a result of the generation of defect states.

[*] M. Moser, Dr. I. Czekaj, Prof. J. Pérez-Ramírez
Institute for Chemical and Bioengineering, Department of Chemistry and Applied Biosciences, ETH Zurich
Vladimir-Prelog-Weg 1, 8093 Zurich (Switzerland)
E-mail: jpr@chem.ethz.ch
Prof. N. López
Institute of Chemical Research of Catalonia (ICIQ)
Av. Països Catalans 16, 43007 Tarragona (Spain)
E-mail: nlopez@iciq.es

Supporting information for this article is available on the WWW under http://dx.doi.org/10.1002/anie.201404022.

 © 2014 Wiley-VCH Verlag GmbH & Co. KGaA, Weinheim

of IrO_2 and RuO_2 for HBr oxidation compared to HCl oxidation is in agreement with a previous study on supported catalysts.[5] As shown in the energy profiles of the reactions over RuO_2 (Supporting Information, Figure S1), the lower energy requirement for Br_2 evolution by recombination of surface bromine atoms, in comparison with that of Cl_2, explains the shift to lower temperature in HBr oxidation. More importantly, the inactivity of TiO_2 in HCl oxidation (no conversion at 723 K) greatly contrasts with its activity in HBr oxidation (over 90% conversion at 673 K). In fact, the conversion profiles of TiO_2 and IrO_2 in HBr oxidation almost coincide. A long-term test over TiO_2 extrudates was performed to assess the stability of the system, a crucial aspect for the prospective application of this material. As shown in Figure 1b, the catalyst in a technical form showed a stable and high space-time yield of bromine over 30 h on stream. The insets of Figure 1b show a significant color change of the solid from the original white to pale yellow after reaction. The coloration can be related to the presence of defect states, which were rapidly introduced by contacting TiO_2 with the HBr oxidation atmosphere. All the changes occurring during reaction affect exclusively the surface of the material. X-ray diffraction shows that the rutile structure of the catalysts was unaltered after exposure to HBr (Figure S2), proving that bulk bromination does not occur.

For an in-depth analysis of the TiO_2 surface, two samples treated in HBr oxidation (code $HBr + O_2$) and in HBr without gas-phase oxygen (code HBr) were investigated by X-ray photoelectron spectroscopy (XPS; Tables S1–S3). The XPS spectra in Figure 2a show the Ti $2p_{3/2}$ region of the fresh and treated samples. All three spectra are very similar and contain a main peak for Ti^{4+} (binding energy, BE = 458.5 eV). The HBr-treated sample shows an approximately 5% contribution of a peak at BE = 457.5 eV attributed to Ti^{3+} and 5–9% of a second peak at BE = 459.8 eV ascribed to Ti_{OH}. This result indicates that some surface oxygen was removed, thus, some of the titanium atoms are in a Ti^{3+} oxidation state. The calculated shifts for XPS (Table S4) further support the appearance of Ti^{3+} species with lower binding energies either by formation of vacancies (1 eV) or by bromination (0.7 eV) both with respect to Ti^{4+}. This is further supported by the O 1s and Br $3d_{5/2}$ spectra (Figure S3, Table S1–S4). Additional information on the surface state can be retrieved from the valence band (VB) of the spectra (Figure 2b). At the top of the VB, the fresh catalyst presents a characteristic feature, around 3 eV. According to the density of states (DOS) obtained with the cluster model representing the stoichiometric surface (Figure 2c, bottom), this feature corresponds to the contribution of two-fold coordinated (bridging) O_b atoms. Upon HBr treatment, this fingerprint smoothens out, Figure 2b. This result is substantiated by the DOS from the oxygen-deficient O_{vac} and the Br_b models represented (Figure 2b blue and red lines and models in Figure 2c middle and top, respectively). Both O_{vac} and Br_b models (Figure 2b blue, green and red dashed lines and models in Figure 2c middle and top, respectively) diminish the intensity of the peak at 3 eV, accounting for the origin of the spectral differences in Figure 2b. Thus, XPS analyses of used rutile provide valuable indications to construct a proper computational model to assess the activity patterns observed in Figure 1a.

The mechanism and energy profile of HBr oxidation over various oxides are shown in Figure 3a. The reaction proceeds as follows: O_2 is activated (Steps 1,2) and, in parallel, HBr is dissociatively adsorbed (Step 3) generating hydroxy groups. These can recombine to form water (Step 4) followed by its desorption (Step 5). Recombination of bromine atoms leading to Br_2 evolution (Step 6) completes the catalytic cycle. HBr adsorption and OH recombination are acid–base reactions, mainly controlled by the total charge of the ions on the surface and thus they are weakly dependent on the particular rutile oxide considered. Differently, O_2 adsorption and Br_2 recombination have a marked redox character as the main species upon adsorption (O_2 or Br) withdraw part of the electronic density from the oxide. Accordingly, it is the specific redox ability of each rutile-type oxide what determines its activity in the oxidation of hydrogen halides. For metallic oxides, like RuO_2 and IrO_2, the redox properties are rather constant but in semiconductors they can be modified to a large extent by doping. Understanding the catalytic role of TiO_2 in HBr oxidation requires the consideration of its complexity. In agreement with previous results,[6,7] O_2 activation on the stoichiometric surface (Steps 1,2) is endothermic by more than 4 eV and thus unfeasible (Figure 3a, green line). However, the surface still maintains its

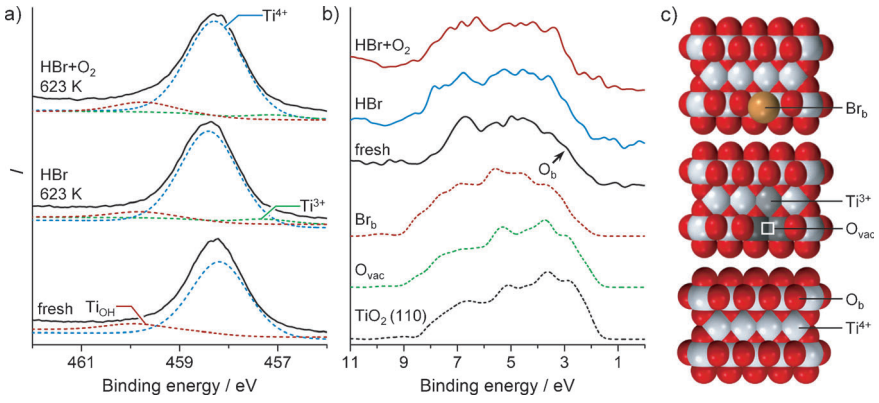

Figure 2. X-ray photoelectron spectra of rutile TiO_2 before and after exposure to different atmospheres. a) Upon treatment in HBr, Ti^{3+} was detected on the catalyst surface in the Ti $2p_{3/2}$ core level spectra. b) In the valence band (solid lines), the signal of oxygen in bridge positions (O_b) was weaker for the samples treated in HBr and $HBr + O_2$. The interpretation of the spectra in (b) by cluster simulations of the TiO_2(110) surface (dashed lines) suggest the formation of oxygen vacancies (O_{vac}) or of the replacement of O_b by bromine atoms in bridge positions (Br_b). c) Top views of various TiO_2(110) clusters. The fresh sample shows a stoichiometric surface, that is, free of defects (bottom). Dissociative adsorption of HBr with subsequent water evolution leads to the formation of an oxygen vacancy (O_{vac}), changing the electronic structure of neighboring titanium atoms (middle). These vacancies are immediately brominated (top). The energy for the bromination process is presented in Figure 3b.

© 2014 Wiley-VCH Verlag GmbH & Co. KGaA, Weinheim

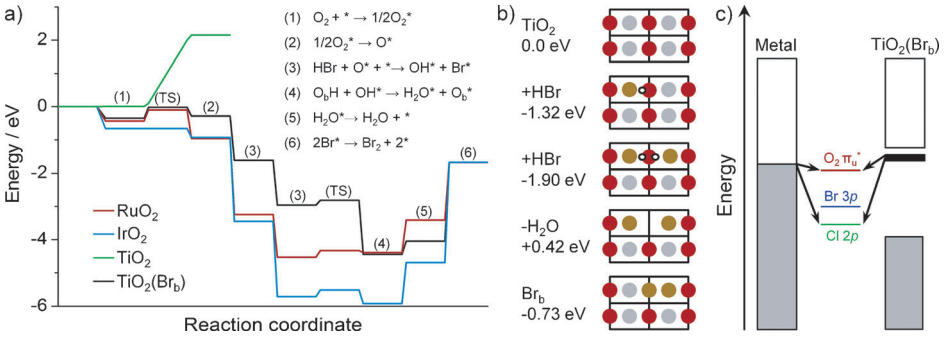

Figure 3. a) Reaction profiles of HBr oxidation over the (110) facet of RuO_2, IrO_2, TiO_2, and Br-containing $TiO_2(Br_b)$. The numbers (1) to (6) refer to the elementary steps depicted in the inset and * to an empty site. The catalytic cycle presented corresponds to $2\,HBr + 1/2\,O_2 \rightarrow Br_2 + H_2O$. b) Bromination path on the TiO_2(110) p(2×1) model: red O, gray Ti, white H, and brown Br atoms. c) Schematic representation of the band diagrams of metal oxides that behave as metals (IrO_2 and RuO_2) and the defect-state containing semiconductor $TiO_2(Br_b)$. The possible injection mechanisms are shown by arrows, where the relative position of the reactant levels highlights the scale of stronger (long arrows) to weaker (small arrows) binding energies.

acid–base properties. Therefore, the heterolytic dissociation of HBr represented by Step 3 can be driven by the basic surface lattice oxygen atoms and the acidic empty Ti_{cus} (cus = coordinatively unsaturated site). The reaction leads to O_bH and Br_{cus} and opens a path to the activation of the surface with the formation of defect states, as illustrated in Figure 3b. After a second HBr molecule dissociates on the surface the two hydroxy groups can recombine to form a water molecule at a bridge position (H_2O_b) with two bromine atoms sitting at Ti_{cus} positions (Br_{cus}). Starting from the clean surface this set of reactions is exothermic by 2 eV. Water can then evolve to the gas phase, leaving a vacancy behind at the bridge position that is rapidly occupied by one of the Br_{cus} atoms that transforms into Br_b. The overall doping process is exothermic by 0.73 eV (Figure 3b) and explains sample coloration (inset of Figure 1b) and the characteristic fingerprints in XPS. Notice that similar chlorination was reported for RuO_2 in HCl oxidation.[9,10] However in TiO_2 and as Br contains one electron more than O, when it replaces the O atom, a defect state with one extra electron is populated. Once doped, oxygen adsorption can occur (Figure 3a, $TiO_2(Br_b)$ black line). Indeed, Step 1 leading to the monohapto molecular adsorption of oxygen is exothermic, by 0.70 eV (1/2 of this value in the reaction profile shown). In parallel, O_2 dissociation, HBr adsorption, OH recombination, and H_2O desorption are relatively easy on the doped titanium oxide sample. The gas-phase evolution of Br_2 by recombination of adsorbed bromine atoms is, as in all the investigated oxides, the most energy-demanding step. The computed energy need for Step 6 on $TiO_2(Br_b)$ (2.36 eV) is higher than that of RuO_2 (1.76 eV) but smaller than that of IrO_2 (3.02 eV).

These energies are decreased by the gas-phase entropy gain (between 1.1–1.6 eV depending on the temperature). For $TiO_2(Br_b)$, Br_2 evolves leaving the self-doped surface behind and completing the catalytic cycle. Upon taking into account competitive adsorption and gas-phase entropy, the DFT results indicate that the activity of $TiO_2(Br_b)$ falls in between that of RuO_2 and IrO_2. Therefore, in line with the experimentally determined apparent activation energy of the rutile-type oxides: RuO_2 (0.46 eV) < TiO_2 (0.56 eV) < IrO_2 (0.81 eV), see Figure S5a. Furthermore, all the catalysts exhibit a strong dependence on the oxygen partial pressure with reaction orders of 0.6 (TiO_2), 0.7 (RuO_2), and 0.8 (IrO_2; Figure S5b). This observation, in good agreement with the results on HCl oxidation, arises from the large barrier for halide evolution that limits the number of active empty positions for surface re-oxidation.[5,9] The competition between oxygen and the halides for the active sites implies that both parameters are relevant to retrieve activity. The catalytic activity of $TiO_2(Br)$ in HBr oxidation can be understood by the level alignment between the material and the reactants. A schematic band diagram is shown in Figure 3c. For the defect-free TiO_2, occupied levels (marked gray) are too deep for charge transfer to O_2 interacting with the surface thus rendering it inactive. Instead, defect states associated with the bromine-doped $TiO_2(Br_b)$ are placed in the band gap close to the conduction band and thus at much higher energies (marked black). These high-energy electrons can then be effectively transferred to O_2, turning oxygen adsorption exothermic (Figure 3a). However, charge transfer also takes place when halides desorb. In Step 6 of the reaction scheme, X_2 desorption implies that the electrons stored in the isolated halide, which is negatively charged, are transferred back to the material. As the electron affinity of Cl is about 0.2 eV higher than that of Br,[11] it forms stronger bonds to $TiO_2(X)$ and requires more energy to evolve Cl_2 ($\Delta E = 3.17$ eV) than Br_2. Cl_2 evolution is much more energy demanding than Br_2 and O_2 adsorption cannot effectively take place at the operating temperature at which formation of gas-phase Cl_2 is effective. This situation results in the zero activity of TiO_2 in HCl oxidation (Figure 1a). Thus, the energy alignment of $TiO_2(X)$ defect states is reasonable for HBr but not adequate for HCl oxidation. This explanation also reveals why SnO_2, also with rutile structure, is inactive for HBr oxidation, as its defect levels are too low in energy to be efficiently transferred to O_2. The O_2 calculated adsorption energy is −0.40 eV, not enough to occur at the temperatures required for Br_2 evolution.

There is a final confirmation of the different origin of activity for TiO_2 when compared to RuO_2 and IrO_2. The variation of the activity for Cl and Br on RuO_2 (or IrO_2) at 60% conversion is approximately 125 K. This is related to the halide evolution (Step 6) that controls the activity through the number of empty sites available for O_2 adsorption.[9a] As both are linked, in principle there is a single electronic parameter, the metal oxide work function, that provides the energy from which electrons are injected and back-donated that determines activity (see Supporting Information, Section S2). However, this behavior is not retrieved for TiO_2, over which

 © 2014 Wiley-VCH Verlag GmbH & Co. KGaA, Weinheim

only HBr can be oxidized. For TiO_2, the adsorption dependence between molecular oxygen and halide adsorption is different than for the metallic oxides (RuO_2 and IrO_2) as a result of different electrostatic contributions. Thus, it is an outlier in the corresponding linear scaling relationships. Indeed, the adsorption energy of O_2 is smaller than it would be for a metallic rutile. This explains why IrO_2 is as active as TiO_2 because the larger barrier for halide evolution is compensated by a very effective O_2 trapping; the molecular monohapto adsorption on IrO_2 is exothermic by 1.32 eV (see Supporting Information Section S3).

The analysis shows when oxidation mechanisms could potentially occur on these materials and how the process is linked to photo-electro-chemical uses of TiO_2 compounds. In the photo-electro-chemical applications, the population of high-chemical-potential electrons is achieved by using photons or a voltage, these high-energy electrons have similar properties to those coming from the self-doping found for the HBr reaction on TiO_2. But this mechanism has some limitations. It does not work if there is a single redox pair (i.e. only oxygen) in the reaction network. The example is CO oxidation, which on TiO_2 occurs by the activation of oxygen at vacancies, thus when the reaction is carried out it completely heals the defects. Once the available surface and near surface vacancies are extracted and filled,[8b] the reaction stops revealing its stoichiometric (non-catalytic) character. Therefore, for a catalytic oxidation to occur on the semiconductor, the doping levels need to be stable under reaction conditions. The long-term stability of the catalyst is difficult to maintain because of the decreasing number of defect states in oxygen-rich environments.[8] However, in $TiO_2(Br_b)$, bromine substitution leaves active defect states in the material but simultaneously blocks the paths for bulk re-oxidation. Therefore, the outstanding stability of titanium oxide in HBr oxidation (Figure 1b) is based on the self-doping character of the reaction. Extended geometrically defective areas, such as steps,[8c] could potentially render defect states for the reaction in a similar manner opening new parallel channels.

In summary, the generation of defect related states in a semiconductor, such as rutile TiO_2, originates an active and stable catalyst for bromine production through HBr oxidation and self-doping. Self-doping can be achieved provided that 1) the determining reaction steps belong to redox couples, 2) the alignment between the levels of the active species and the defect states favor the adsorption/desorption process, and 3) the defect states are preserved during the reaction. The preservation of defect states guarantees the long-term stability of the material and the scope for practical application. Our results warn against considering theoretical models that are too simple when addressing the properties of oxides and the possibilities of doping in semiconducting oxides. To our knowledge, this is the first use of rutile TiO_2 as an active phase in heterogeneously catalyzed processes, and besides the remarkable HBr oxidation performance, the low cost and abundance of the material should be highlighted. The large-scale implementation of TiO_2 can be done using recently developed fixed-bed technology for HCl oxidation, an adiabatic reactor cascade with intermediate heat exchange and HBr feeding (Figure S6a). Figure S6b in the Supporting Information illustrates the temperature profile, HBr conversion, and the O_2:HBr ratio along the six reactors filled with TiO_2. The modular design allows the optimization of the bromine production by manipulation of the reactor inlet temperatures and/or the HBr feed streams. The simulated case demonstrates the production of approximately 1.7 tons of bromine per day using only 9 kg of rutile TiO_2.

Experimental Section

Catalyst testing and characterization: RuO_2 and IrO_2, were prepared by calcination of anhydrous $RuCl_3$ (Alfa Aesar, 99.99%) and $IrCl_3$ (ABCR, 99.9%), respectively, at 823 K for 5 h (heating ramp = 5 K min^{-1}). Rutile TiO_2 (Aldrich, nanopowder, 99.5%) was calcined identically prior to its use. TiO_2 extrudates (diameter = 2 mm, length = 4 mm) containing 80 wt.% rutile and 20 wt.% anatase were prepared following the method described elsewhere.[9b] The rutile-type metal oxides in particulate form (particle size = 0.4–0.6 mm, 0.25 g) and the extrudates (1 g) were evaluated in the gas-phase oxidation of HX (X = Br, Cl) in a continuous-flow fixed-bed reactor with 8 mm or 17 mm i.d., respectively. Steady-state tests were conducted at ambient pressure using a total flow of F_T = 166 cm^3 STP min^{-1}, feed mixtures with 10 vol.% HX, 5–60 vol.% O_2, balanced in N_2, and temperatures of T = 420–740 K. X_2 at the reactor outlet was quantified by iodometric titration using a Mettler Toledo G20 compact titrator. The conversion of HX was determined as X_{HX} = 2 mole X_2 at the reactor outlet/1 mole of HX at the reactor inlet × 100. The space-time yield is defined as STY = grams of Br_2/(hour×gram of catalyst). The catalysts were collected after rapid quenching of the reactor to room temperature in N_2 flow and characterized by X-ray diffraction (PANalytical X′Pert PRO-MPD). X-ray photoelectron spectroscopy (VG Thermo Escalab 220i-XL, Al K_α source, UHV 10^{-9} mbar) was carried out over TiO_2 samples after reaction for 5 h at 623 K in O_2:HBr = 0.25, 1, 2 (HBr + O_2), and 0 (pure HBr). The samples were prepared and transported in the nitrogen atmosphere. The XPS spectra were charge corrected with respect to the C 1s signal (i.e. 284.5 eV).

Computational details: Density functional theory as implemented in the VASP was applied to slabs representing the (110) facets of RuO_2, IrO_2, and TiO_2.[12] The exchange-correlation functional was PBE,[13] and for TiO_2 PBE + U, U_{eff} = 4.5 eV. Inner electrons were replaced by PAW,[14] and monoelectronic valence states were expanded in plane waves with a cutoff energy of 450 eV, spin polarized calculations were performed when needed. The supercell employed was a (2 × 2) containing five trilayers ($OTiO_2O$ motif). In optimization the two bottom layers were fixed. The k-point sampling was 5 × 3 × 1. Transition states were identified by CI-NEB.[15] Cluster calculations were performed using StoBe and $Ti_{21}O_{64}H_{44}$ model[16] only neighboring centers to Br_b or oxygen vacancies were reoptimized.

Received: April 5, 2014
Published online: June 2, 2014

Keywords: defects · heterogeneous catalysis · hydrogen bromide · oxidation · titanium oxide

[1] G. Pacchioni, *ChemPhysChem* **2003**, *4*, 1041 – 1047.
[2] a) U. Diebold, *Surf. Sci. Rep.* **2003**, *48*, 53 – 229; b) M. Grätzel, *Nature* **2001**, *414*, 338 – 344; c) X. Chen, S. S. Mao, *Chem. Rev.* **2007**, *107*, 2891 – 2959.
[3] a) K. Seki, *Catal. Surv. Asia* **2010**, *14*, 168 – 175; b) J. Pérez-Ramírez, C. Mondelli, T. Schmidt, O.-F. Schlüter, A. Wolf, L. Mleczko, T. Dreier, *Energy Environ. Sci.* **2011**, *4*, 4786 – 4799.

 © 2014 Wiley-VCH Verlag GmbH & Co. KGaA, Weinheim

[4] a) E. McFarland, *Science* **2012**, *338*, 340 – 342; b) K. Ding, H. Metiu, G. D. Stucky, *ChemCatChem* **2013**, *5*, 1906 – 1910.
[5] M. Moser, L. Rodríguez-García, A. P. Amrute, J. Pérez-Ramírez, *ChemCatChem* **2013**, *5*, 3520 – 3523.
[6] A. Toftelund, I. C. Man, F. Abild-Pedersen, T. Bligaard, J. Rossmeisl, F. Studt, *ChemCatChem* **2012**, *4*, 1856 – 1861.
[7] H. Metiu, S. Chrétien, Z. Hu, B. Li, X. Sun, *J. Phys. Chem. C* **2012**, *116*, 10439 – 10450, and references therein.
[8] a) M. Setvin, U. Aschauer, P. Sheiber, Y.-F. Li, W. Hou, M. Schmid, A. Selloni, U. Diebold, *Science* **2013**, *341*, 988 – 991; b) N. López, J. D. Prades, F. Hernandez-Ramirez, J. R. Morante, J. Pan, S. Mathur, *Phys. Chem. Chem. Phys.* **2010**, *12*, 2401 – 2406; c) R. Bechstein, H. H. Kristoffersen, L. B. Vilhelmsen, F. Rieboldt, J. Stausholm-Møller, S. Wendt, B. Hammer, F. Besenbacher, *Phys. Rev. Lett.* **2012**, *108*, 236103.
[9] a) D. Teschner et al., *J. Catal.* **2012**, *285*, 273 – 284; b) M. Moser et al., *ACS Catal.* **2013**, *3*, 2813 – 2822, see Supporting Information.
[10] a) D. Crihan et al., *Angew. Chem.* **2008**, *120*, 2161 – 2164; *Angew. Chem. Int. Ed.* **2008**, *47*, 2131 – 2134.
[11] N. N. Greenwood, A. Earnshaw, *Chemistry of the Elements*, 2nd ed., Elsevier, Dordrecht, **2008**, p. 800.
[12] a) G. Kresse, J. Furthmüller, *J. Comput. Mater. Sci.* **1996**, *6*, 15 – 50; b) G. Kresse, J. Furthmüller, *Phys. Rev. B* **1996**, *54*, 11169 – 11186.
[13] J. P. Perdew, K. Burke, M. Ernzerhof, *Phys. Rev. Lett.* **1996**, *77*, 3865 – 3868.
[14] P. E. Blöchl, *Phys. Rev. B* **1994**, *50*, 17953 – 17979.
[15] G. Henkelman, B. P. Uberuaga, H. J. Jónsson, *J. Chem. Phys.* **2000**, *113*, 9901 – 9904.
[16] a) I. Czekaj, J. Wambach, O. Kröcher, *Int. J. Mol. Sci.* **2009**, *10*, 4310 – 4329; b) K. Hermann et al., StoBe-deMon, deMon Software, Stockholm, Berlin, **2005**, see Supporting Information.

 © 2014 Wiley-VCH Verlag GmbH & Co. KGaA, Weinheim